ASPECTOS DO USO DE CO2 SUPERCRÍTICO NO PROCESSO DE SEQUESTRO POR MEIO DE MECANISMOS DE MINERALIZAÇÃO

O IMPACTO DA EXECUÇÃO DE WAG PARA O AUMENTO DA EFICIÊNCIA DO PROCESSOD E MINERALIZAÇÃO COM CO2 SUPERCRÍTICO

Water Alternating Gas Cycling to Optimize CO_2 Mineralization for Geological Carbon Storage: Cascadia Project

I. Demirkanli[1], S. White[1], M. White[1], A. Bonneville[1],and D. Goldberg[2]

Pacific Northwest NATIONAL LABORATORY

Proudly Operated by Battelle Since 1965

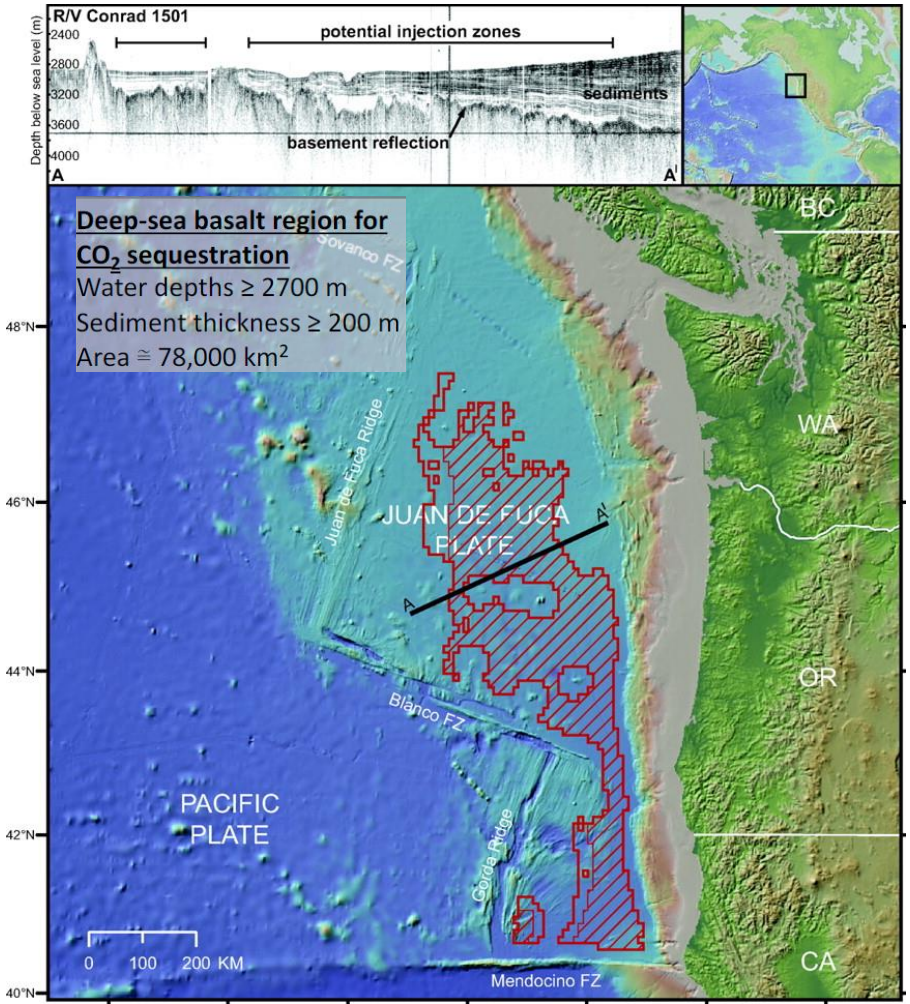

O IMPACTO DA EXECUÇÃO DE WAG PARA O AUMENTO DA EFICIÊNCIA DO PROCESSOD E MINERALIZAÇÃO COM CO2 SUPERCRÍTICO

- **STOMP-CO_2 w/ ECKEChem**

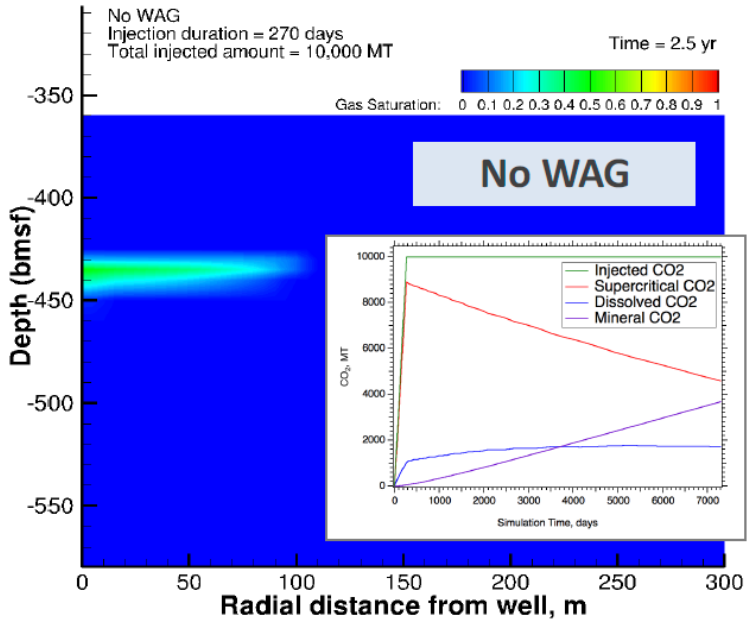

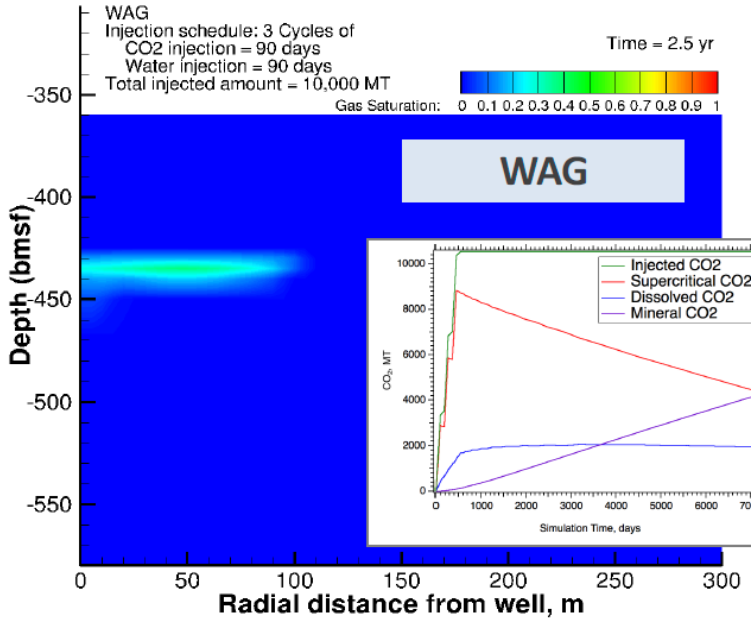

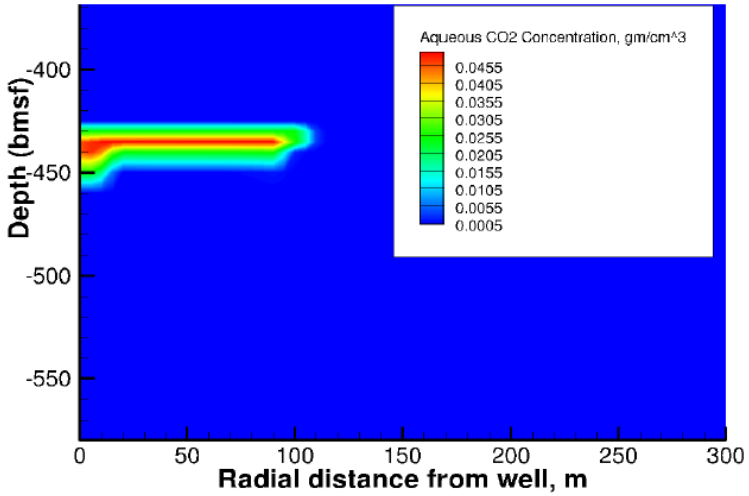

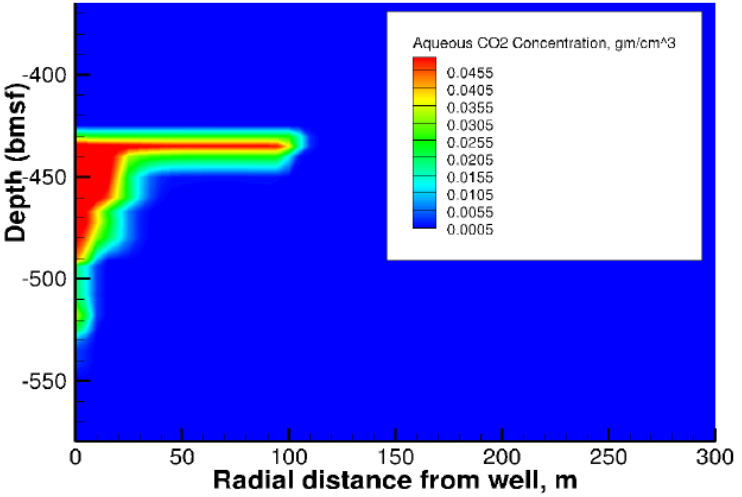

Heliyon 8 (2022) e09635

Contents lists available at ScienceDirect

Heliyon

journal homepage: www.cell.com/heliyon

Research article

Simulation of carbon dioxide mineralization and its effect on fault leakage rates in the South Georgia rift basin, southeastern U.S.

Adil Alshammari [a,*], Venkat Lakshmi [b], Duke Brantley [a], Camelia C. Knapp [c], James H. Knapp [c]

[a] School of the Earth, Ocean, and Environment, University of South Carolina, United States
[b] Department of Engineering Systems and Environment, University of Virginia, United States
[c] School of Geology, Noble Research Center, Oklahoma State University, United States

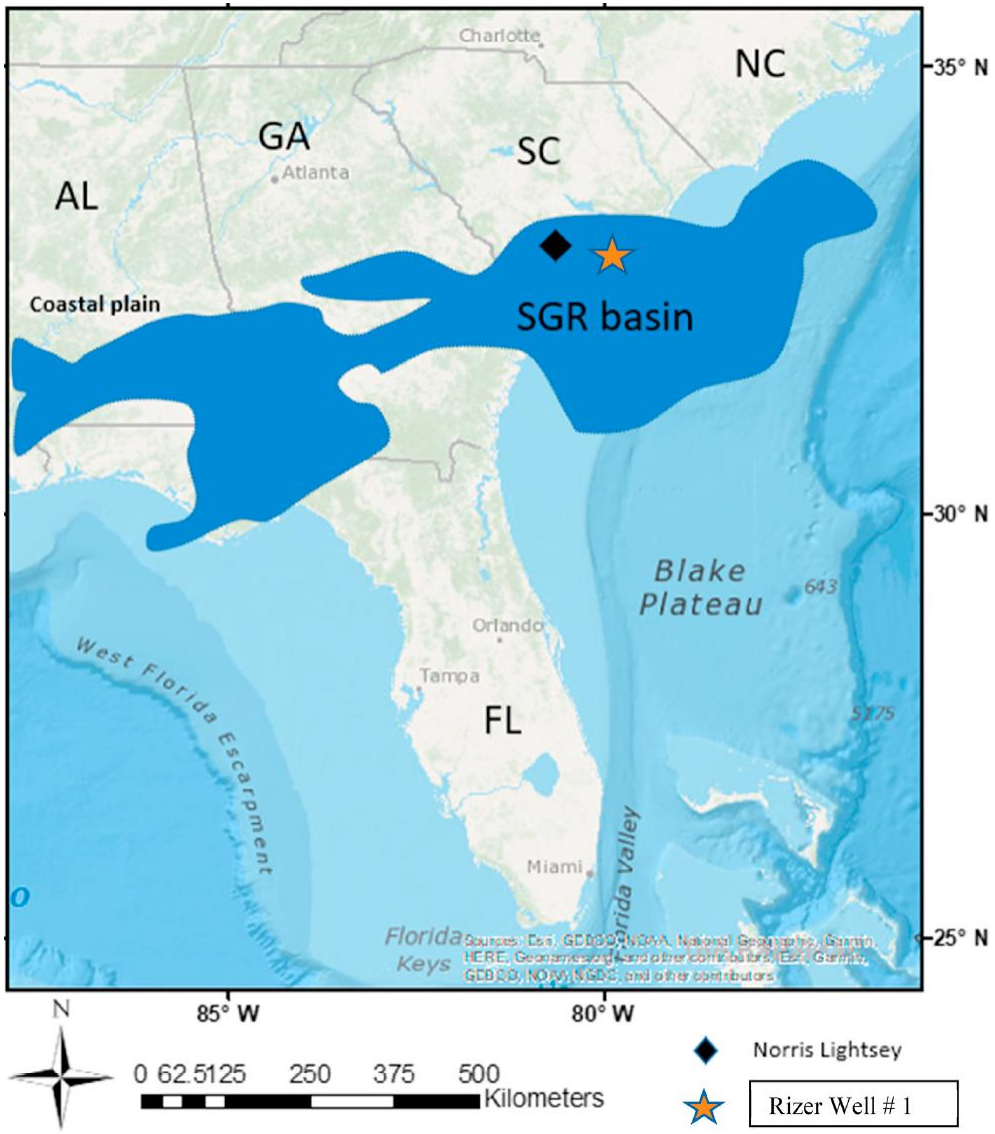

South Georgia Rift Basin

Stratigraphic distribution of the Norris Lightsey #1 borehole

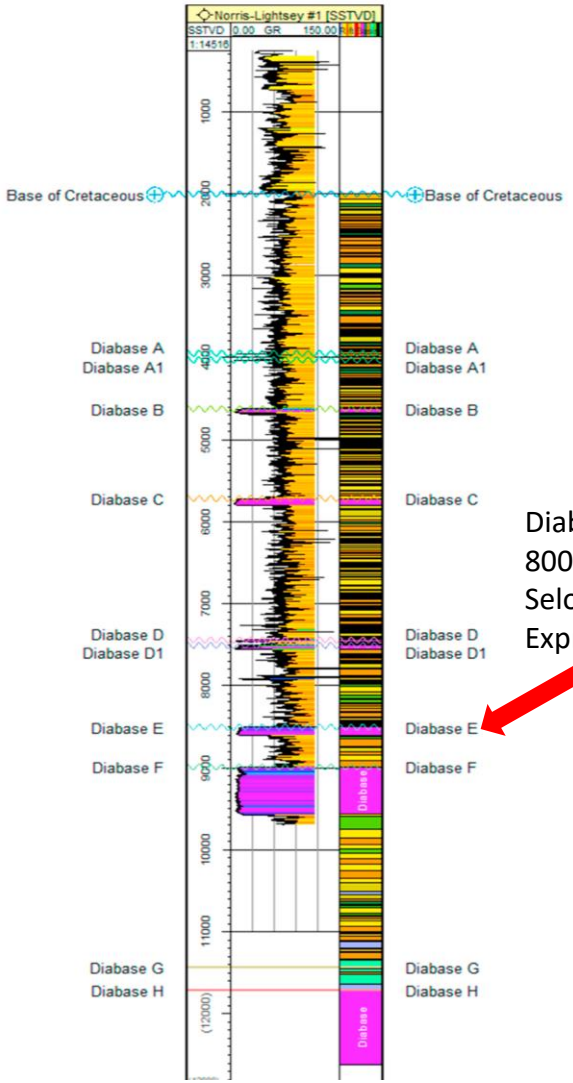

Diabásio E
800 m profund
Selo de arenito
Expressão aerial

Rochas vulcânicas (Jurássico) intercaladas com arenitos (red beds – Triássico)

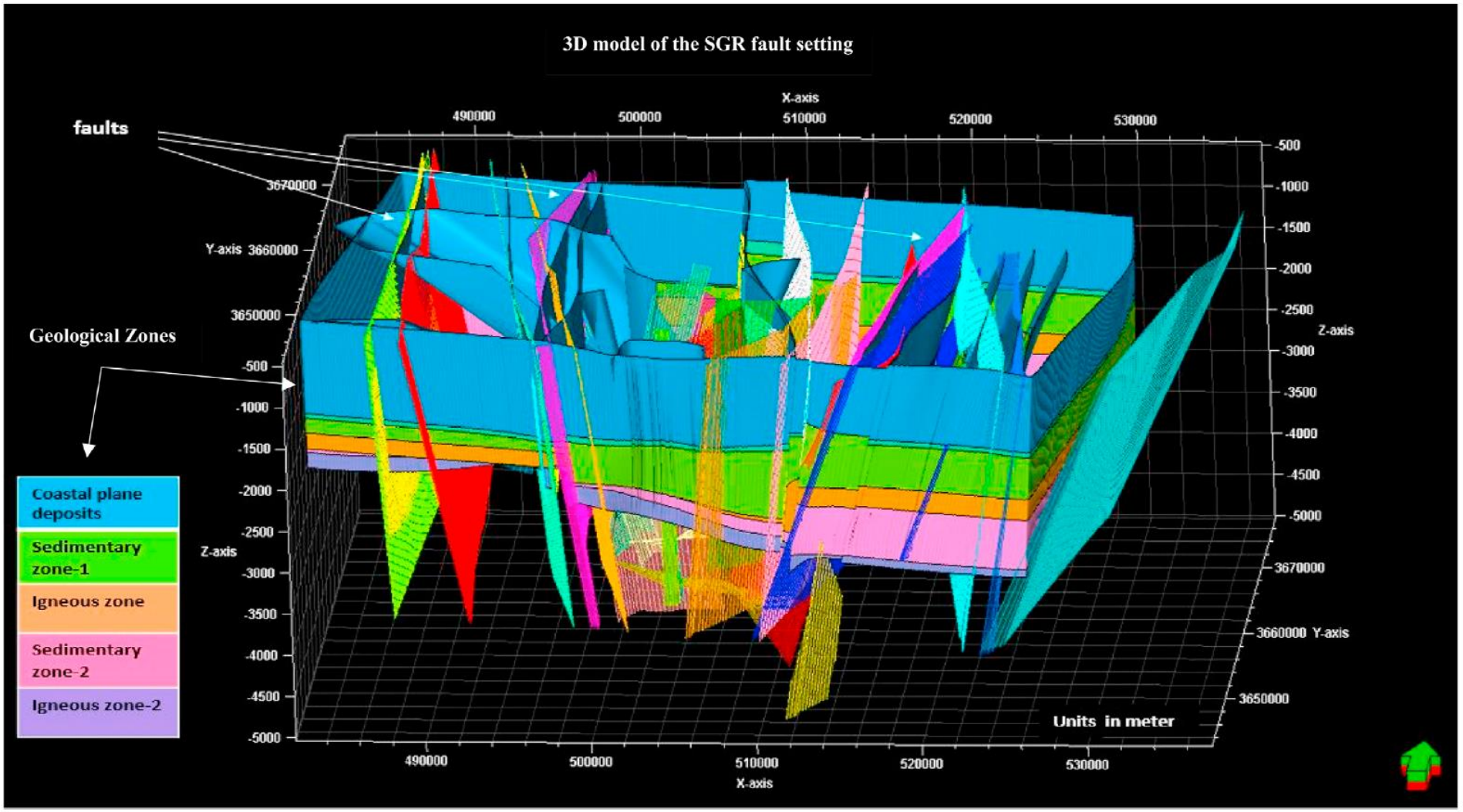

Figure 3. 3D model of the SGR displaying the orientation of faults, density, and the complexity of the geological settings due to tectonic activities. This figure was generated using Petrel 2014 software by analyzing the seismic and borehole data. The figure was modified from Brantley et al., (2015).

A

3D- Model of SGR basin

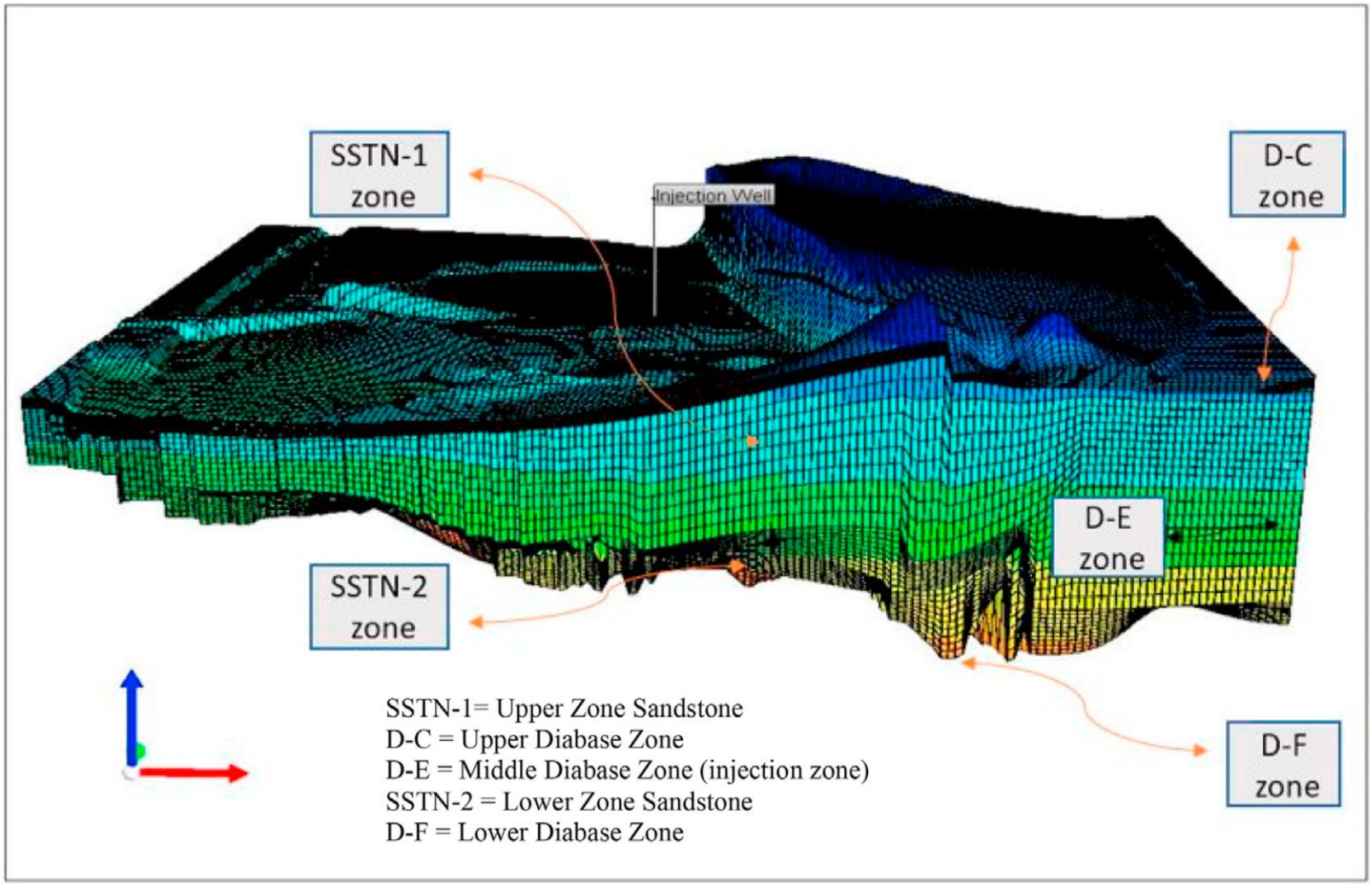

B

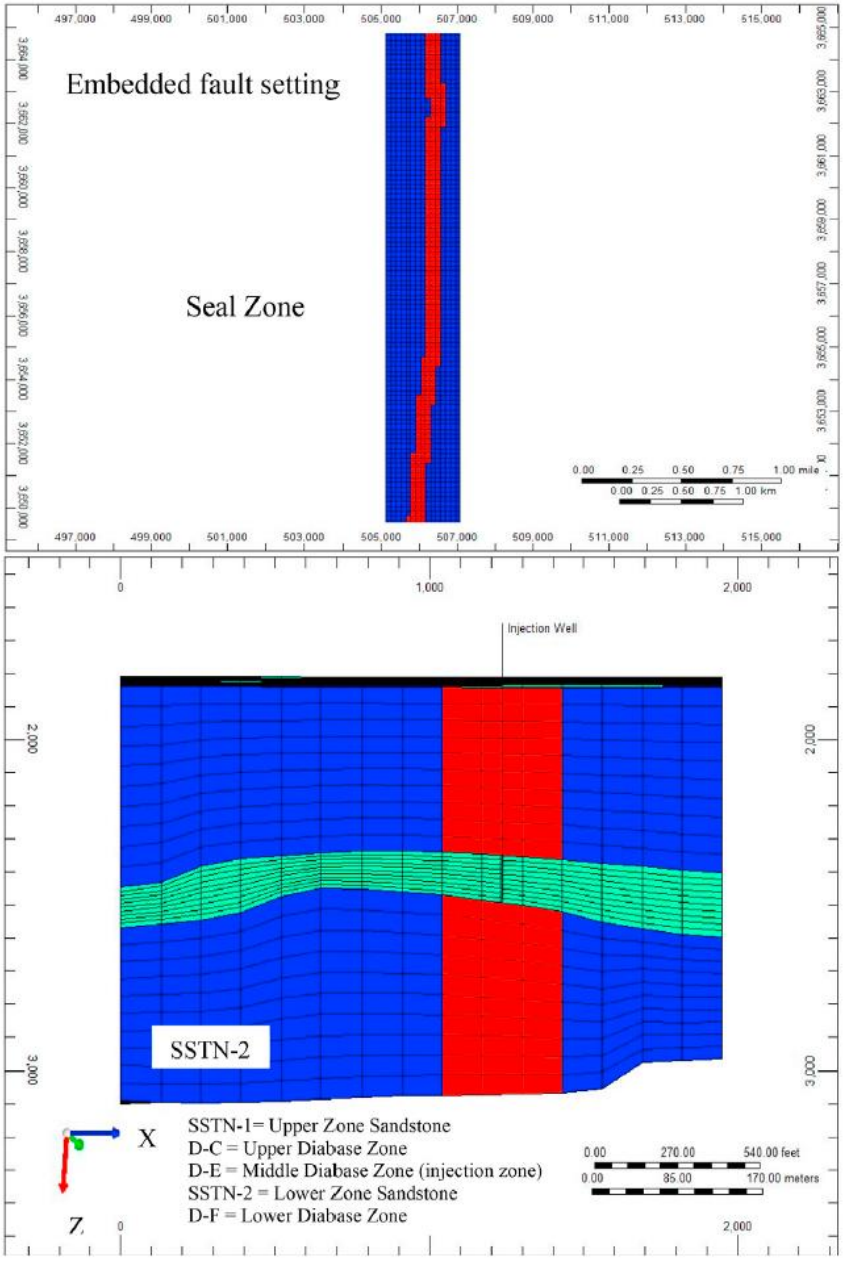

Figure 4. A. 3D CMG-model of the SGR basin. The SGR model was divided into five zones from top to bottom (D-C, SSTN-1, D-E, SSTN-2, D-F). The injection zone (D–E) was located in the middle of them model and surrounded vertically by two seal zones (SSTN-1 and SSTN-2). The model was comprised of a sequence of igneous and sedimentary rocks. B. 2D depiction of the location of embedded fault within the simulation model. The top view (X–Y) shows the fault indicated by red located between the top seal comprised of sandstone indicated by the blue area in the figure. The side view shows the red fault zone crossing the blue seal zones and green injection zone vertically. The area within the fault zone applied various permeability values during each simulation. The location of the injection well was placed close to the crest of anticline of the injection zone (D–E) to avoid the lateral migration of CO_2.

The 3-D simulation model used the CMG, 2017 software package was built using the following settings (Figure 4A and Table 1):

1. Five zones that started at a minimum depth of 1200m. Each zone included ten layers. The first (D-C), third (D-E), and fifth (D-F) zones had a wide range of igneous rock while the second (SSTN-1) and fourth (SSTN-2) zones were characterized by sedimentary rock. This classification was compatible with the sequences of sedimentary and igneous strata.
2. The sedimentary zones SSTN1 and SSTN2 were considered to be seal zones while the igneous zone D-E was considered to be an injection zone as it is surrounded vertically by two seals (Figure 4A and Figure 4B). All of these horizontal zones were intersected vertically with a range of permeability values for the fault zone.
3. The average porosity and permeability of sedimentary rocks that served as seals for the model were 0.34% and 0.00065 mD, respectively. For igneous rocks (the reservoir part of the model), porosity and permeability were designated to be 14% and 10 mD, respectively, as they have been affected by prior erosion and tectonic activities to a greater extent than the sedimentary rocks (Akintunde et al., 2013). The injection zone had a scaled permeability (from 0 to 200 mD) to reflect the heterogeneity of the petrophysical features and to match the lateral variability.
4. The fault permeability zone ranged from 0.1 mD (which provided the maximum resistance) to 1000 mD (which provided the minimum resistance) to cover the heterogeneity that exists in the basin.
5. CO_2 was injected in all layers of the third zone (D-E) where the zone intersected the fault.
6. The initial conditions at the top of the model were adjusted to 30 °C and 55 MPa or 8000 psi for temperature and pressure, respectively. This is will change during the injection period(Figure 5).
7. The simulation period started during the year of 2016 and extended to 2216. The volumetric injection rate of CO_2 was 10 M m^3/year of supercritical CO_2 over 20 years. The well injection was then shut down, and the fate of the CO_2 was predicted though the simulation to 2216.
8. The resolution of the model was 172 by 148 grids for the 50 layers and covered the area around the fault.

Taxa de injeção 10 M m^3/ano ao longo de 20 anos

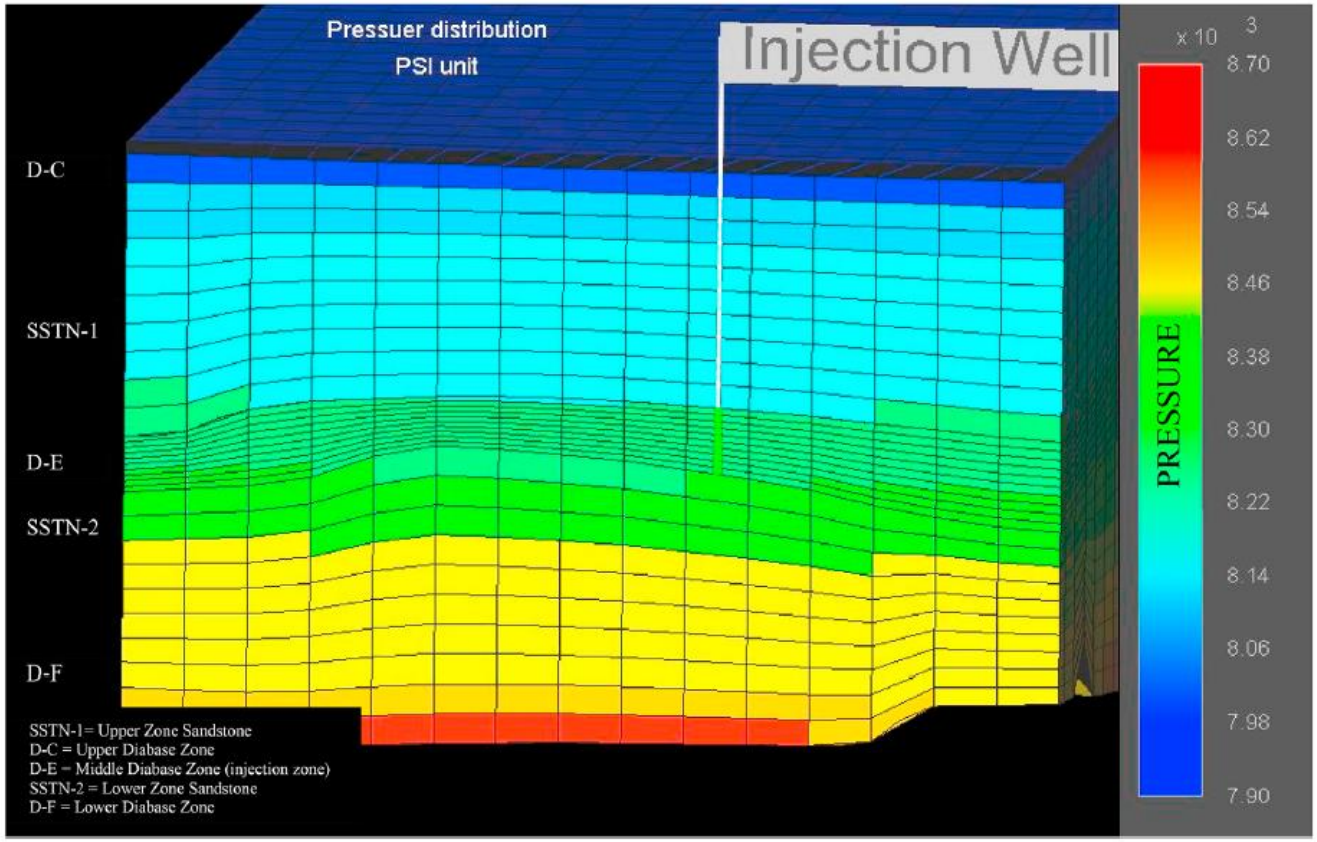

Figure 5. Pressure distribution of the model at initial conditions. The pressure at the bottom of the simulation model was 7.9 × 10^3 PSI which was equivalent to cumulative pressure in the beginning of simulation. The model was located at an approximate depth of 2000 m and the pressure at the injection zone was 8400 PSI.

Table 1. Parameters for model simulation in SGR Basin. Each zone has ten layers and porosity and permeability values. The top of the model is Diabase –C while the bottom of the model is Diabase –F. The injection zone is Diabase -E, and the seal zones are sandstone one and two zones.

Injection simulation Model Set Up					
Material/Zone	50-layer total in the Model	Depth (m)Min/Max	Porosity (%)	Permeability (mD)	Notes
Diabase C	Layer 1-10	1283/1916	14	10	Top of model
Sandstone 1	Layer 11-20	1387/2848	3.4	0.00065	Seal
Diabase E	Layer 21-30	1710/2953	14	1-200 range	Injection Horizon
Sandstone 2	Layer 31-40	1710/3453	3.4	0.00065	Seal
Diabase F	Layer 41-50	1710/3517	14	10	Base of Model

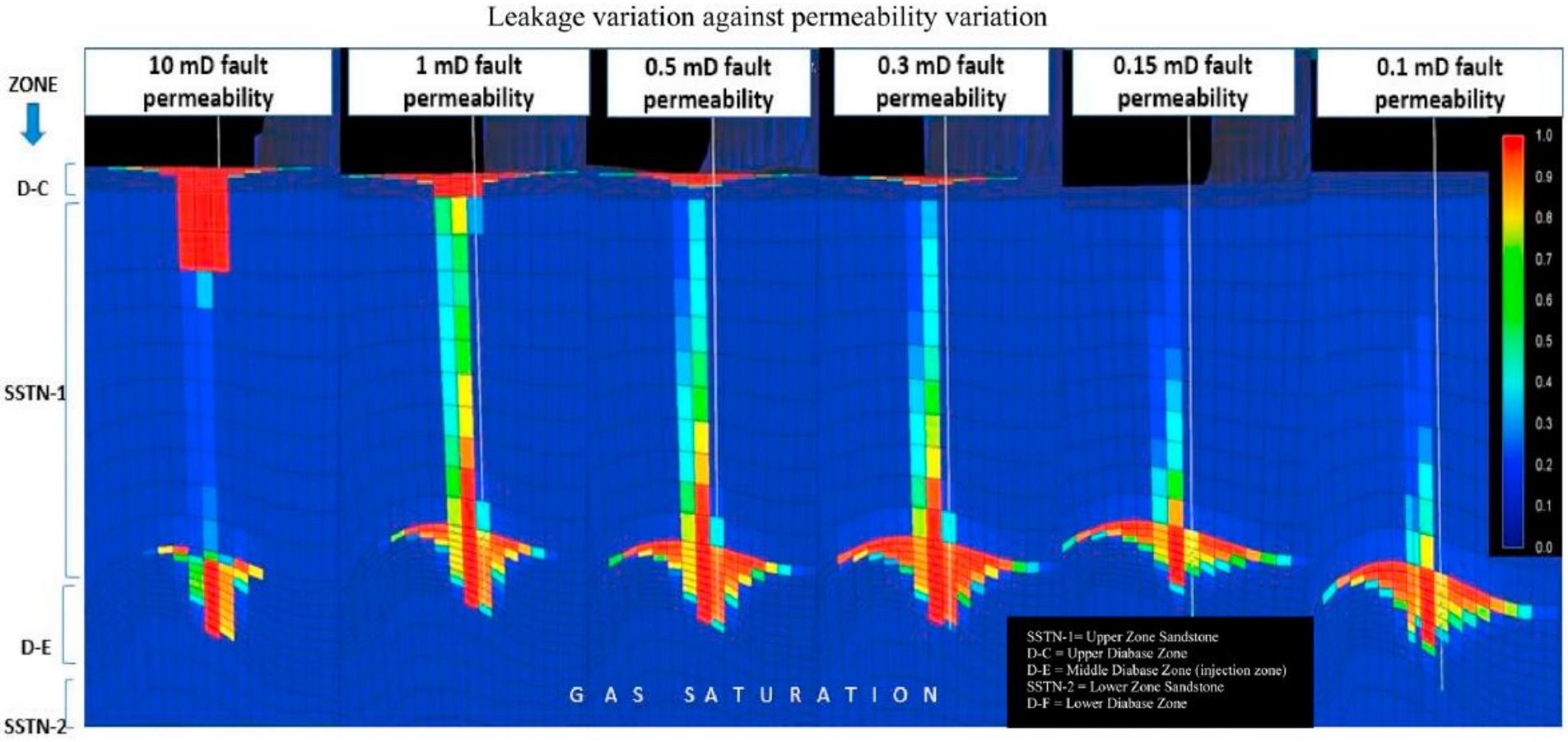

Figure 6. Display of selected models with respect to fault permeability at the end of the simulation time (year = 2100) in the case of no mineralization. Applying the simulation showed that resistance was inversely proportional to the fault permeability value. The higher fault permeability values showed a lower resistance to CO_2 migration. The gradient of color reflects the CO_2 saturation in the model. Models for higher values of permeability show that a part of the CO_2 plume rose to the top of the model as a result of low resistance of the seal zone SSTN-1. For the permeability of 0.1 mD, CO_2 almost failed to penetrate the upper seal. In contrast, permeabilities greater than or equal to 0.3 mD allowed CO_2 to pass the seal zone SSTN-1.

Modelagem Química Aplicada

Table 2. Composition of geochemical minerals modified from (Xiong et al., 2018) Grand Ronde Basalt Sample Composition

Mineral	Composition (vol %)	Formula
plagioclase	58	Ca0.51 Na0.46 K0.03 Al1.47 Si2.49 O8
pyroxene	14	Mg0.72Fe0.59Ca0.60Si1.90Al0.12O6
ilmenite	3	FeTiO3
glass	25	Si0.98Al0.02Na0.008K0.002Ca0.002Fe0.001O2

Table 3. Six models have been applied in simulation against selected values of fault permeability and reflect a time sequence for first appearing at the top layer of the 3D model as an indicator of the speed of migration, the 10 mD F.p. In case 1, the migration time is fast to arrive at the top layer of (D-C) in 2025 from the simulation start time in 2016 and graded as a weak resistance. While the value 0.1 in case 6 gave the maximum time that extended at the end of the simulation time in 2116 and graded as a Full resistance (No – Vertical Migration).

Case No.	Fault permeability (mD)	First, arrive at the top of the model	Resistance	Notes
1	10	2025	Weak	
2	1	2037	Low	
3	0.5	2052	medium	
4	0.3	2067	Good	
5	0.15	2105	Very Good	
6	0.1	———	Full	No indicator for immigration until end of the simulation

When mineralization was simulated in this model, it demonstrated supercritical CO_2 injection within the reservoir D-E between two seal zones SSTN-1 (top) and SSTN-2 (bottom). During this process, a chemical reaction was expected to occur between the CO_2 and igneous rocks in the injection zone starting immediately when CO_2 mixed with formation water to dissolution occurs (Gislason et al., 2014). The chemical reactions that lead to mineralization were adjusted by WINPROP software, a part of the CMG package 2107 software, which considered the chemical parameters in Table 4 according to Eqs. (1), (2), (3), (4), (5), and (6).

Equations:

$$CO_2\,(g) + H_2O \leftrightarrow H_2CO_3^{-} \quad (1)$$

$$H_2CO_3 \leftrightarrow (H^+) + (HCO_3^-) \quad (2)$$

$$2Mg_2SiO_4 + CO_2 + 2H_2O = Mg_3Si_2O_5\,(OH)_4 + MgCO_3 \quad (3)$$

$$Mg_3Si_2O_5\,(OH)_4 + 3CO_2 = 3MgCO_3 + 2SiO_2 + 2H_2O \quad (4)$$

$$(Ca^{++}) + (HCO_3^-) = CaCO_3 + H^+ \quad (5)$$

$$5(H_2O) + 2(Al^{+++}) + 2(SiO_2(aq)) = Al_2Si_2O_5(OH)_4 + 6H^+ \quad (6)$$

Distribuição de Calcita

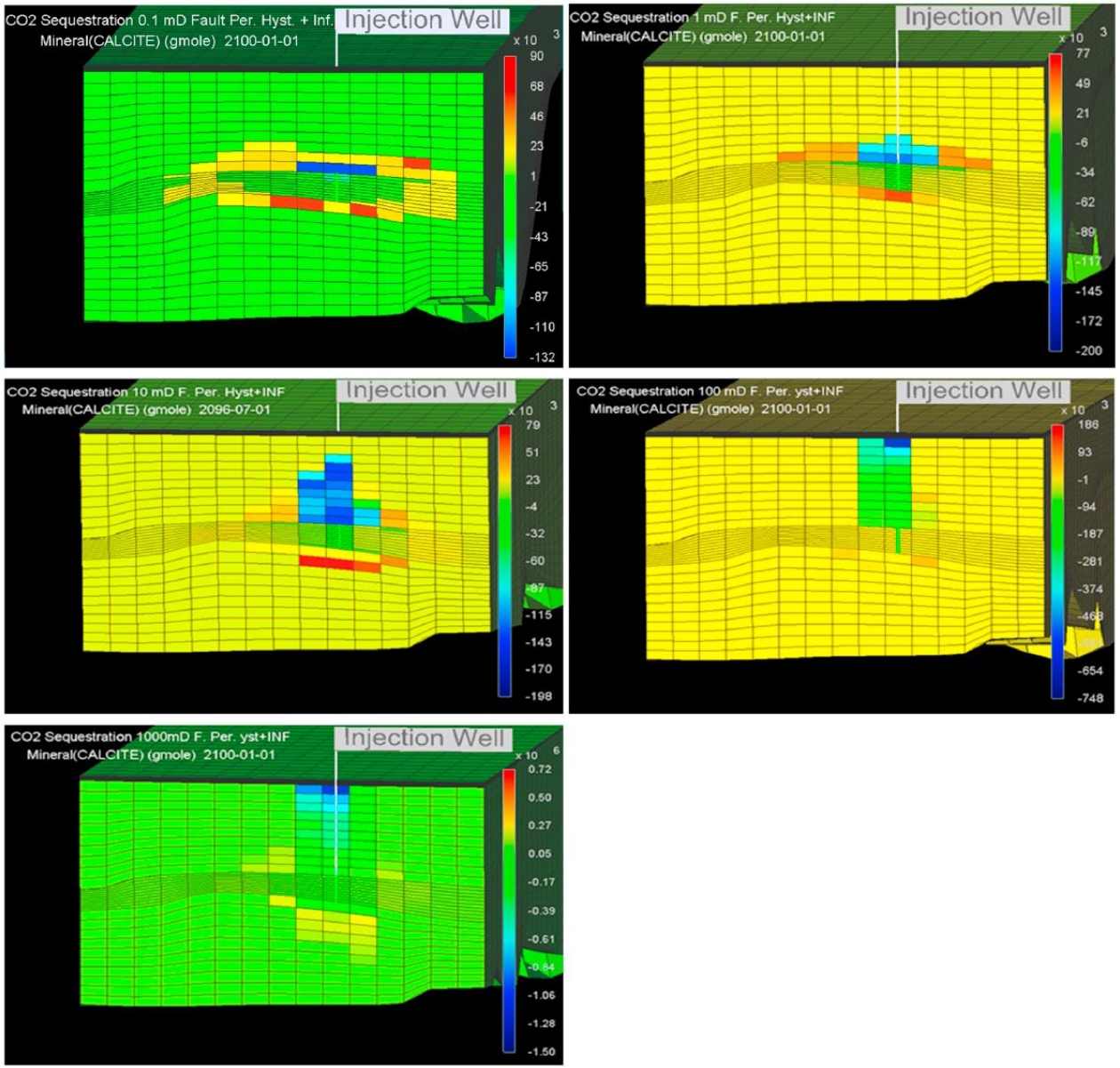

Figure 10. Impact of fault permeability on calcite distribution. This figure shows calcite distribution for the logarithmic scale of permeability and highlights the associated migration patterns. For the wide range of permeability values applied the results were polarized as only widespread leakage or no leakage was observed. Although mineralization occurred, it is difficult to control the plume migration.

A simulação mostrou a formação de caolinita em todos os ranges de permeabilidade da falha

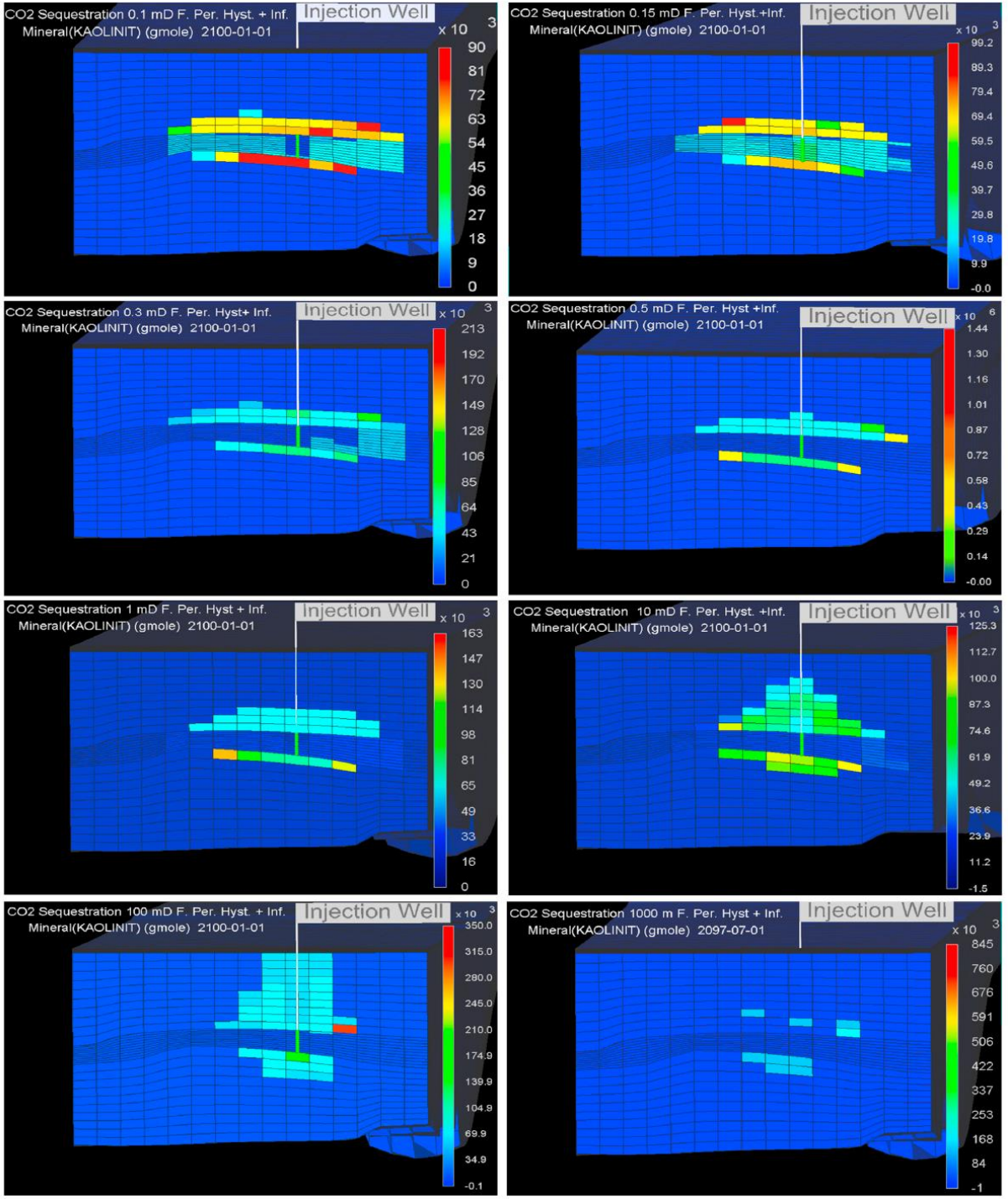

7.3. Kinetic reactions

Contrary to what was found in the Rizer #1 borehole, it was assumed in the model that there was sufficient basaltic rock and formation water available so that these factors were not limiting for mineralization. Because no information could be found to support volcanic activities in the SGR Basin, temperature variation was assumed to be negligible and a constant temperature was used. The rate of a chemical reaction varied depending on permeability since there was a limited and constant injection rate of 10 million m^3/year of supercritical CO_2. At the beginning of the injection, the supercritical CO_2 mixed with the formation's water and formed the previously described dissolved phase. Meanwhile, the supercritical CO_2 in the formation continued to increase during injection to a maximum value of 2.27 E09 mole at 2036. During the injection period, the pH increased rapidly as indicated in Figure 16. Then, the amount of supercritical CO_2 in the formation decreased and was impacted by fault permeability, especially in the seal zones (Figure 17). The dissolution of supercritical CO_2 doubled between fault permeability 0.1 and 1000 mD, dissolving 1.5 E09 moles and 3 E09 moles of CO_2, respectively. The maximum dissolution value with respect to time in each zone illustrated that permeability impacted the CO_2 plume's migration (Table 5). Following the dissolution of CO_2, in the chemical reactions described in Eqs. (1), (2), (3), (4), (5), and (6) the solubility of CO_2 increased and was proportional to permeability in every zone except the injection zone. In the injection zone, fault permeability was inversely proportional to dissolution due to the horizontal movement of CO_2 related to the seals' high resistance (Table 5). In Eqs. (1),

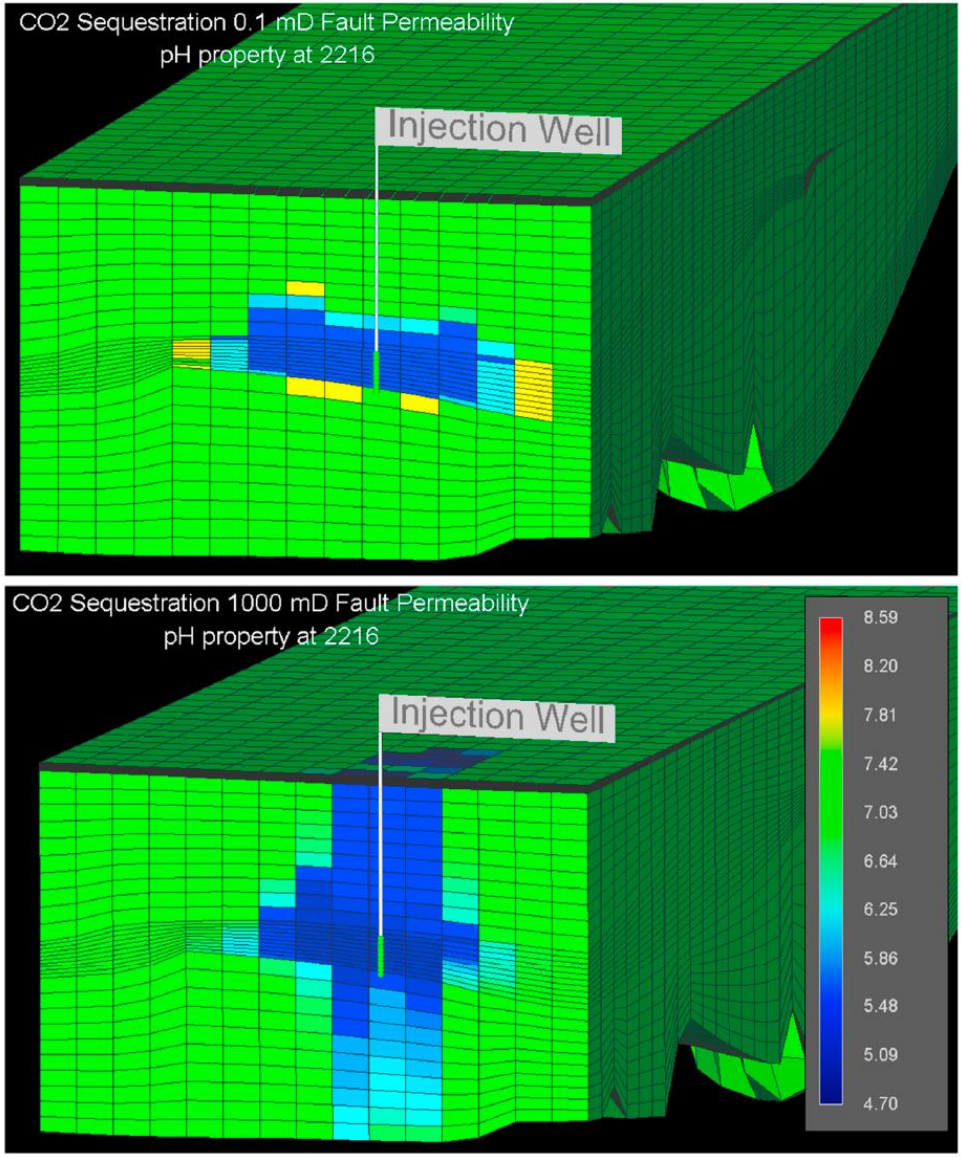

Figure 16. Acidity of 1000 mD fault permeability model. This figure shows the distribution of pH in the CO_2 plume. The upper seal SSTN-1 showed a higher acidity and was similar to that observed at injection zone D-E. This is because a large permeability allows the CO_2 plume to move up due its specific gravity, particularly in the case of the 1000 mD permeability model.

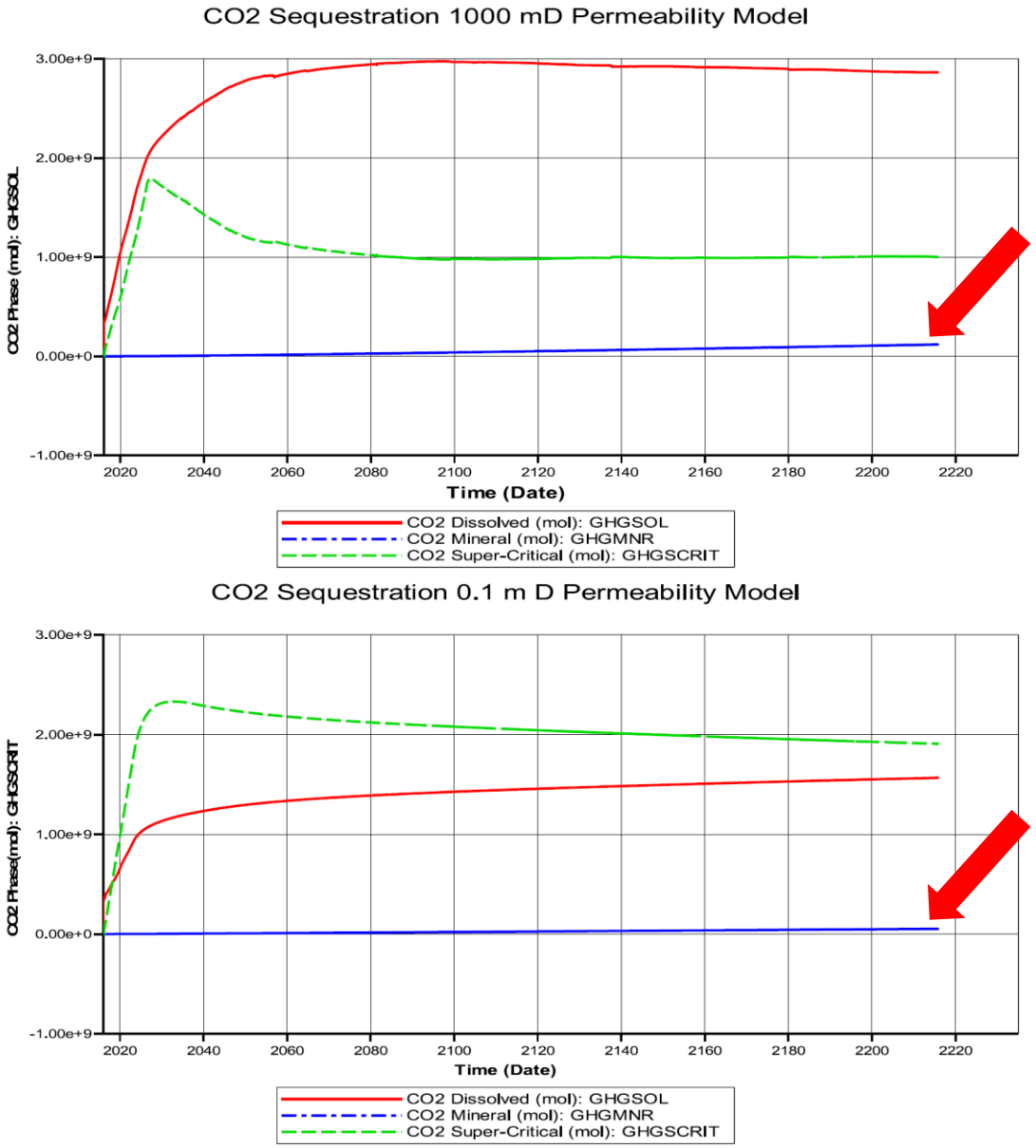

Figure 17. Distribution of the CO_2 phases over time for fault permeabilities values 0.1 mD and 1000 mD.For the fault permeability 0.1 mD, the seal effectively kept the supercritical CO_2 within the injection zone and its migration was horizontal. In this scenario, the dissolved CO_2 phase increased rapidly during the injection period and remained constant after injection through the end of simulation. For 1000 mD fault permeability, the seal allowed CO_2 to leak out of the injection zone. For this case, the maximum value of supercritical CO_2 was still low relative to that of the 0.1 mD case and double the amount of dissolved CO_2 for 0.1 mD case (2.97 EXP +09 mol vs. 1.55 EXP +09 mol). Mineral phase CO_2 in the case of 1000 mD was more than 0.1. However, most of the CO_2 in the mineral phase was observed outside of the injection and seal zones due to the low resistance of the seal zone.